APPLICATION OF MAGNETIC FIELDS IN INDUSTRIAL GROWTH OF SILICON SINGLE CRYSTALS

W. von Ammon[1], *Yu. Gelfgat*[2], *L. Gorbunov*[2], *A. Mühlbauer*[3], *A. Muiznieks*[4], *Y. Makarov*[5], *J. Virbulis*[6], *G. Müller*[7]

[1] *Siltronic AG, 24 Johannes Hess Str., 84489 Burghausen, Germany (wilfried.ammon@siltronic.com)*
[2] *Institute of Physics, University of Latvia, 32 Miera, LV-2169, Salaspils, Latvia*
[3] *Institute for Electroheat, University of Hanover, 4 Wilhlem-Busch-Str., D-30167 Hanover, Germany*
[4] *Faculty of Physics and Mathematics, University of Latvia, 8 Zellu street, LV-1002 Riga, Latvia*
[5] *Semiconductor Technology Research, Inc., P.O.Box 70604, Richmond, VA 23255-0604, U.S.A.*
[6] *PAIC, Riga, LV-1002, 8 Zellu street, Latvia*
[7] *Department of Material Science (WW6), Crystal Growth Laboratory, University of Erlangen-Nürnberg, 7 Martensstr., D-91058 Erlangen, Germany*

Introduction. The use of magnetic fields for the growth of semiconductor crystals has already been considered many decades ago. As early as in 1966, Chedzey et al. [1] and Utech *et al.* [2] reported about InSb crystals grown in a horizontal boat under the influence of a magnetic field. They found a suppression of temperature fluctuations in the InSb melt and a decrease of growth variations (striations) in the crystal. In 1970, Witt *et al.* [3] applied a static transverse (horizontal) magnetic field to the Czochralski (CZ) growth of InSb crystals. 10 years later, in 1980, the transverse field was also used for the CZ growth of silicon single crystals [4, 5]. Since then, the method has received considerable attention over the years. One of the major driving forces for introducing magnetic fields in the industrial CZ growth of silicon crystals was the request by the semiconductor industry to replace floating zone (FZ) grown crystals which had been the preferred material for the manufacturing of high power devices [6]. The reason for this changeover was the fact that the FZ method in the early 80's could not follow the rapid crystal diameter increase as required by the industry, namely, the switch from 4" to 5" diameter. The application of magnetic fields to the CZ technique (MCZ) allowed the growth of low-oxygen crystals which had similar properties as the FZ grown crystals.

After the MCZ technology had been established as a standard method for low- oxygen CZ material, it was found that magnetic fields were also useful for the growth of advanced CZ crystals, e.g., the so-called "perfect", "pure" or "ultimate" silicon [7, 8, 9]. Silicon crystals of this type are grown under conditions which avoid large agglomerates of intrinsic point defects, i.e., Lpits (Si interstitial aggregates) and voids (vacancy aggregates). Below a critical size, these defects are no longer harmful to device functioning and, hence, can be tolerated. Today, a substantial part of the CZ pullers are equipped with a transverse magnetic field of 3000 to 5000 G, which has been shown to be most suitable for the production of this advanced material.

In most cases, static magnetic fields have been preferred up to now, but, in recent years, dynamic magnetic fields were also investigated as they have a number of advantages which will be discussed below.

The paper briefly reviews different types of magnetic fields applied to CZ and FZ silicon crystal growth and their impact on process stability and crystal quality. It is also intended to appreciate and highlight the very fruitful and successful collaboration in this field between the above authors and their institutes over now almost one decade.

1. Czochralski crystal growth.

1.1. Magnetic fields in CZ crystals growth. The CZ method, which was originally developed by Jan Czochralski [10], uses a crucible to hold the melt from which the crystal is grown (Fig. 1). The only suitable crucible material for silicon crystal growth is silica (SiO_2). The growing crystal as well as the crucible are rotated – usually conter-rotated – around a common axis. The melt flow field in the crucible, mainly driven by buoyancy and centrifugal forces, is rather complicated. Marangoni forces only have some impact at the local convection near the growth interface at the crystal rim and the trijunction melt/gas ambient/crucible wall. Thin shear layers develop at the crystal-melt and the crucible-melt interfaces. A typical convection pattern is shown in Fig. 2. Due to the cylindrical heater which surrounds the crucible, the hot melt moves upward near the crucible wall, while, below the crystal center, the melt flow is directed downward. It should be noted that, in particular for large melt volumes (charge sizes larger than ca. 25 kg), the melt convection is highly turbulent and, consequently, strongly time dependent [11], i.e., the picture in Fig. 1 has to be understood as an averaged convection pattern over time. The most important growth parameters are crystal and crucible rotation rates, but also the hot zone which determines the temperature field around the crucible and in the growing crystal must be carefully designed. The temperature field, namely, the axial temperature gradient $\mathbf{G}$ in the crystal at the growth interface, has a major influence on the type of defects that develop in the crystal during the cooling phase. It was shown by V.V. Voronkov [12] that the parameter V/G (V = pull rate) controls the type of grown-in defects: if $V/G > \xi_{\text{tr}}$ ($\xi_{\text{tr}} = 0.13$ mm^{2}min^{-1}K^{-1}), vacancy aggregates (voids) develop and,

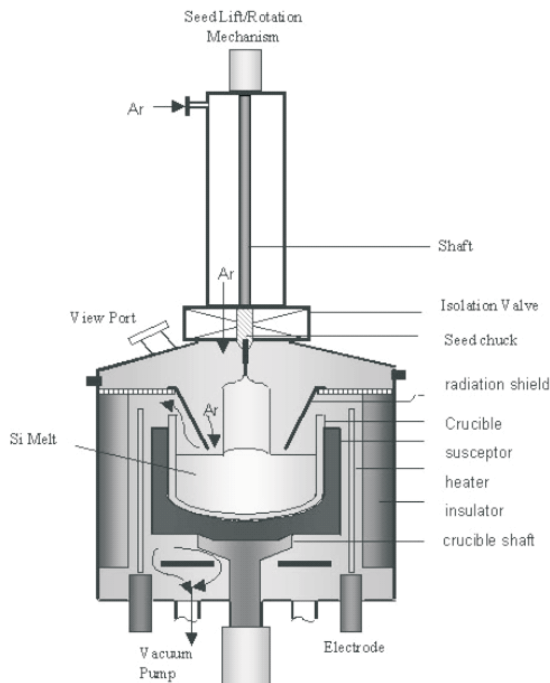

Fig. 1. Czochralski (CZ) puller with a typical hot zone set up.

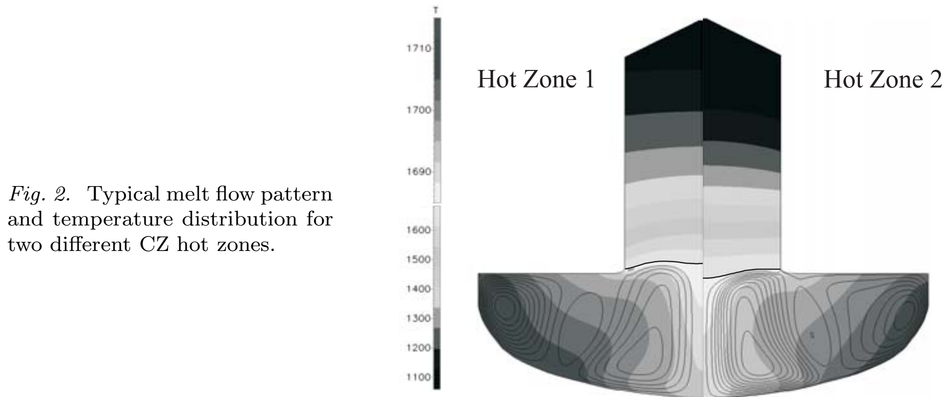

Fig. 2. Typical melt flow pattern and temperature distribution for two different CZ hot zones.

for $V/G < \xi_{\mathrm{tr}}$, Si interstitial related defects (Lpits) are observed. In standard hot zones, **G** exhibits a considerable variation in the radial direction. It is, therefore, not always easy to obtain crystals which contain only one type of defect.

As liquid silicon is highly electrically conductive, magnetic fields have a substantial influence on the melt convection due to the Lorentz force $\mathbf{j} \times \mathbf{B}$, where $\mathbf{j} \sim \mathbf{v} \times \mathbf{B}$ in case of static fields. Static fields mainly slow down the melt convection and, as a result, can damp temperature fluctuations, if the field strength is sufficient, – usually several 1000 G. An important effect of static magnetic fields is also observed on the boundary or shear layer at the growth (crystal-melt) interface [13]. The thickness of this layer increases with a higher field strength which, according to the Burton, Prim and Slitcher (BPS) theory [14] affects the incorporation of impurities into the growing crystal. Magnetic fields may, therefore, have pronounced effects on the axial and radial dopant distribution in the crystal.

Predominantly 3 different types of static fields have been intensively investigated during the last two decades (Fig. 3) [15]. The first type is a simple one coil axial field (early 70ties) which was rather easy to realize around the cylindrically shaped growth furnaces [16, 17]. However, the axial field turned out to be rather unfavorable as it was found that the melt convection exhibits instabilities over wide parameter ranges. In addition, the radial dopant homogeneity is insufficient [15, 18, 19]. Thus, this type of field is only rarely used.

The currently most frequently applied field is probably the transverse or horizontal field [6, 20]. The transverse field particularly suppresses the melt flow in the vertical direction. As a result, the downward flow in the center below the crystal is decreased [21]. However, the overall convection pattern appears to be rather complex. Owing to the asymmetry of the field, computer simulations of the melt flow yield unsatisfactory results and melt convection is therefore only poorly understood. The asymmetry also entails a non-symmetric melt flow and

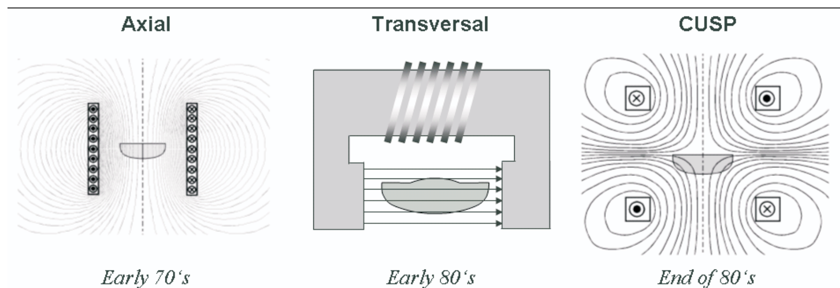

Fig. 3. Different static magnetic field configurations as used for CZ crystal growth.

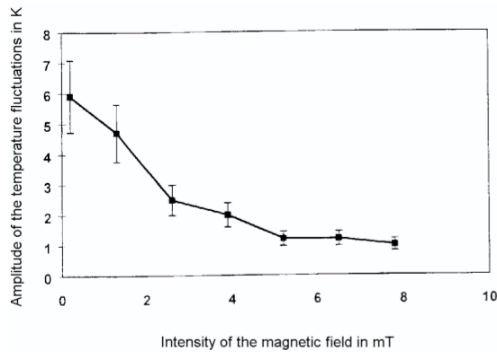

Fig. 4. Damping of temperature fluctuations by dynamic magnetic fields.

temperature field which causes pronounced dopant striations [22]. In the early 80's, when transverse fields were introduced in silicon crystal growth, large and heavy yokes had to be used to obtain the necessary field strength (2000–5000 G). A milestone was, therefore, the development of suitable superconducting magnets for CZ pullers [23] which are smaller in size and consume much less energy. However, the price for such magnets is rather high. Another problem are the stray fields which must comply to the specific safety regulation of the respective country, where the pullers are operated. Furthermore, special care has to be taken that the main cylindrical heater, surrounding the crucible, is not deformed owing to the Lorentz force, which is generated by the electric current in the heater, and the strong magnetic field.

A special configuration is the so-called cusp field [24, 25], where two axial coils generate two opposite fields. The resulting overall field has a minimum in the space between the two coils. It is, therefore, possible to grow the crystal in a nearly field-free environment, while the crucible walls are exposed to a large field strength. The advantage of this field configuration is that the melt convection is close to the growth interface and at the crucible wall can be controlled by separate parameters which often avoids agonizing compromises, e.g., between the adjustment of the required oxygen content and the optimization of its radial variation.

In contrast to static magnetic fields, dynamic magnetic fields, up to now, have only rarely been investigated for crystal growth processes [26, 27, 28, 29]. The driving force is also the Lorentz force, but $\mathbf{j} \sim \mathbf{v} \times \mathbf{B}$ has to be replaced by $\mathbf{j} \sim \boldsymbol{\omega}\mathbf{B}$. Instead of slowing down the melt convection, they specifically drive and, therefore, stabilize a specific melt flow pattern. Consequently, temperature fluctuations are also considerably reduced, as shown in Fig. 4. An important feature of the dynamic fields is the fact that the stabilization of the temperature can be achieved at much lower field strengths (ca. 100 G) if compared to static fields. This translates into smaller size and lower cost of the magnets. The smaller size usually allows to upgrade existing pullers with a magnetic field system without the need to make compromises due to space limitations. There are numerous configurations for the dynamic fields ranging from a simple one coil axial system to a three coil travelling field or even a rotating field with multiple horizontal coils (Fig. 5). As the melt flow is actively driven, many different flow patterns can be realized depending on the field configuration. In case of dynamic fields, the Lorentz force is independent of the melt flow velocity, which makes it easier to avoid instabilities of the convection pattern if compared to some of the static field configurations.

1.2. Challenges in CZ crystal growth. Magnetic fields, as they are applied today, only influence the melt convection. We will, therefore, restrict our discussion to those challenges and problems of CZ crystal growth which may be remedied by an appropriate control of the melt convection in the crucible.

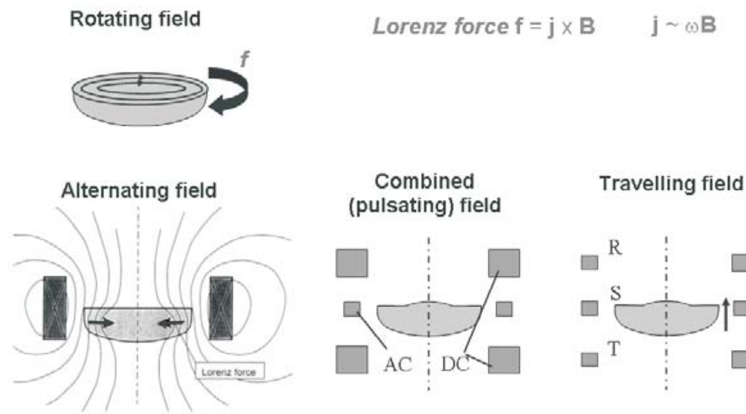

Fig. 5. Dynamic field configurations as applied to CZ crystal growth.

One important issue is the generation of dislocations during the growth process. This is particularly bad for large diameter crystals as a single dislocation rapidly multiplies which generates extensive slippage extending back roughly one diameter into the already dislocation free grown material. Thus, in case of 300 mm crystals, as much as 30 cm of the crystal is rendered useless a dislocation occurs. The cause of dislocations is manifold, e.g., pitting corrosion at the inner surface of the silica crucible which injects particles into the melt, particles in the gas ambient, but also temperature fluctuations of low frequency. As mentioned above, the latter can be effectively suppressed by appropriate magnetic fields, either static or dynamic. The suppression of temperature fluctuations is particularly useful during the growth of the Dash neck after dip in of the seed crystal [30]. The pitting corrosion was found to depend only marginally on the application of magnetic fields, although, they have a notable impact on the temperature at the crucible wall. Static fields tend to increase the temperature at the crucible wall, while dynamic fields usually have the opposite effect. On the other hand, the oxygen concentration at the crucible wall is higher for static fields which decreases the silica dissolution and may compensate the effect of higher temperature. If, however, pitting corrosion is not negligible, static fields can slow down the drift velocity of injected particles so that they have less chance to reach the growth interface. In this case, dynamic fields, which enhance convection, are not a good choice.

A further real challenge has been the growth of "perfect" silicon. This advanced material has come in use as the shrinking design rule of semiconductor devices is approaching or is already less than the size of the built-in vacancy aggregates (< 100 nm). Thus, they have a severe impact on device functioning and, hence, can no longer be tolerated. The manufacturing of "perfect" silicon requires the control of the parameter V/G within very tight tolerances (few percent) over the entire crystal volume during the growth process. Consequently, the radially varying axial temperature gradient $\mathbf{G}$ must be homogenized in the radial direction. As $\mathbf{G}$ is predominantly determined by the design of the upper part of the hot zone (i.e., the heat shield which surrounds the growing crystal), it was first tried to achieve the radial homogenization by reducing the heat loss of the growing crystal at its outer rim close to the growth interface. Although some progress was observed, the results were not satisfying. It was then realized that the melt convection just below the growth interface also has a significant influence on $\mathbf{G}$ and, hence, cannot be neglected. It is necessary to radially homogenize the heat transfer from the melt to the growth interface as well. This can obviously be achieved in a satisfactory way by the application of a transverse field.

Another issue is the twisting of the growing crystals at higher pull rates or fast crystal rotation rates. In particular, 300 mm crystals tend to develop this spiral growth mode. It is closely related to **G** – the higher **G**, the faster the crystals can be grown without the risk of twisting. **G**, in turn, is linked to the lateral temperature gradient G_{ms} on the melt surface at the growth interface. In a simple approach, it was assumed that the radial symmetry of G_{ms} forces the crystal to grow with a cylindrical shape [31]. In this case, it also appears reasonable that there might be a critical value for G_{ms}, below which such cylindrical growth is no longer possible. This model, however, only works sufficiently well as long as the melt convection is not significantly modified. If magnetic fields are applied, maximum pull rates often change in a way which does not fit into this simple picture. For example, the location of the zero field point of the cusp field below or above the melt level has a substantial influence on the critical pull rate at which twisting starts. A similar effect is observed when the direction of a travelling field is reversed. In all cases, the impact on G_{ms} is marginal. Although, a thorough understanding of this behavior is still missing. It is experimentally verified that magnetic fields can be useful to increase pull rates.

One of the major challenges in CZ crystal growth is the adjustment of the oxygen content in the growing crystal according to customer specifications. The technical relevance of the oxygen content stems from the capability of oxygen precipitates to get metallic impurities which are unintentionally introduced during the device process in the bulk of silicon wafers. A further advantage of oxygen doping is the improvement of the mechanical strength of the wafer which avoids slippage during device processing. Common oxygen concentrations range from 3.5 to 8.5×10^{17} atoms/cm^3. The oxygen incorporation in the growing crystal is essentially determined by the evaporation of SiO from the free melt surface, the dissolution rate of the wetted crucible surface – the actual source of oxygen, – and the melt convection. As the ratio between the free melt surface and the wetted crucible surface increases with decreasing melt volume, one would principally expect lower oxygen concentrations at the tail of the grown crystal. However, it turns out that the influence of the melt convection is usually dominant which makes the prediction of the oxygen content very difficult. The latter is a consequence of the fact that a highly turbulent melt convection is strongly fluctuating with time and cannot be simulated with the required accuracy (see below). A satisfactory solution of this complex situation has not yet been found and, thus, the adjustment of the required oxygen content is still often done by trial and error rather than by theoretical calculations. As magnetic fields strongly modify the melt convection, they also have a dominant influence on the incorporation of oxygen into the growing crystal. Although, there are also other means for the oxygen adjustment like the argon ambient pressure and flow as well as the hot zone design, neither of them can change the oxygen content over such a wide range (factor of 2 – 3) as magnetic fields. In particular, oxygen concentrations below 4.5×10^{17} at/cm^3 can usually not be achieved by standard hot zones and processes. However, the magnetic field configuration must be carefully selected with regard to the desired oxygen level. Static fields are useful for low concentrations, as the slowed down melt convection reduces the oxygen transport from the crucible wall, where oxygen is introduced into the melt, to the growth interface. On the other hand, dynamic fields, which enhance the melt flow, often have the opposite effect.

1.3. Simulation of CZ melt convection. The simulation of melt convection in industrial CZ growth processes has become a prerequisite for an economical and timely development of new or improved processes. Owing to the large charge sizes – 350 kg and more are common for 300 mm growth processes – each ex-

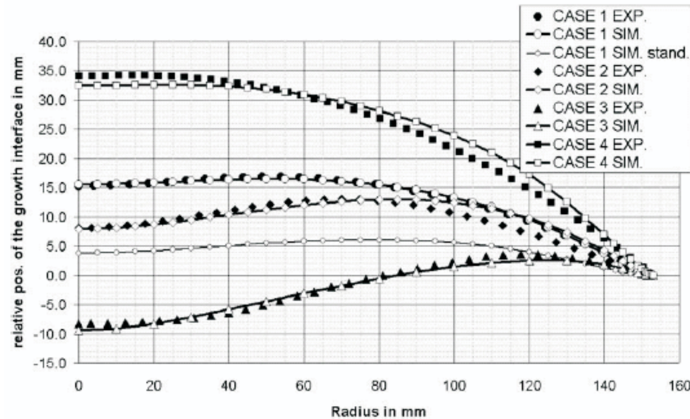

Fig. 6. Comparison of various simulated shapes of growth interfaces with experimental data for different CZ growth processes [37].

periment costs more than 20 T€. Hence, it is mostly too expensive to try to achieve progress by trial and error. In addition, special processes, e.g., the growth of "perfect" crystals, inherently have a rather small process window for numerous parameters which need to be tightly controlled. In these cases, the use of well designed computer simulations is indispensable. Unfortunately, the prediction of melt convection in real CZ systems is a tedious task. It has been demonstrated that the melt convection can only be correctly described by 3D calculations despite the radial symmetry of the environment [32, 33], which drastically increases computer time consumption. The highly turbulent melt flow which generates the unsteady convection pattern further increases computation times. Moreover, turbulence is still an unresolved issue in hydrodynamics and has to be modelled and adjusted to each specific hydrodynamical situation.

In principal, the most promising method for adequately modelling 3D time dependent melt convection would be direct numerical simulations (DNS) which solve the Navier–Stokes equations and the respective boundary conditions without any turbulence models. But these calculations are extremely time consuming due to the enormous number of required grid cells and, thus, have been applied only to small systems up to now [34]. They are currently not feasible for industrial scale CZ growth processes. It appears that the large eddy simulation (LES) technique using grids with a moderate number of computational cells can be a suitable compromise between the potentially rather accurate DNS calculations and standard k-ε models [35]. The latter are much simpler but often reproduce the melt convection in an unsatisfactory way. Although, LES does not resolve small vortices and boundary layers usually have to be modelled by wall functions, they can indeed reveal many important features of the unsteady melt motion. Furthermore, it is possible to combine LES with 2D global models [36] which are well established for predicting heat and mass transfer in the hot zone of a CZ puller. These 2D global models are used to provide the necessary boundary conditions at the various interfaces of the melt volume. However, LES is still too time consuming for engineering solutions. As a consequence, considerable efforts are undertaken to develop 2D axisymmetric approaches which are based on standard k-ε or low Reynolds k-ε turbulence models. Recent investigations, which model the mixing effect of the unsteady melt flow in the region below the growing crystal by an appropriate averaging over time, yielded rather promising results in reproducing the widely varying growth interface shapes for different CZ processes (Fig. 6) [37]. Despite this remarkable success, the accuracy is sometimes still not sufficient. In

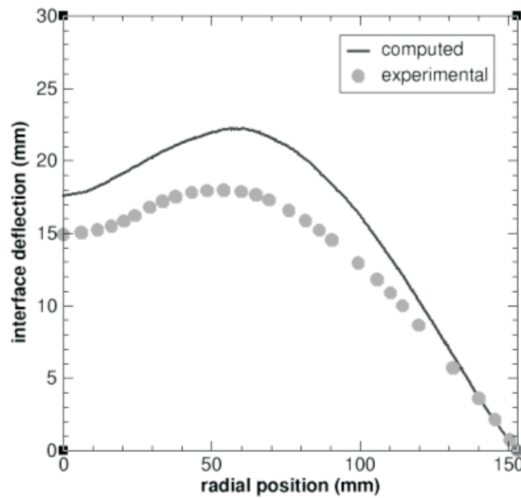

Fig. 7. Comparison of a simulated shape of the growth interface with experimental data for the application of a cusp field to a 300 mm CZ growth process.

particular, when certain growth parameters or the thermal environment are drastically changed, the interface shape and the temperature gradients in its vicinity are often in disagreement with experimental results. A complicated problem is also the calculation of the correct SiO evaporation rate which impacts the oxygen content in the crystal as the argon gas flow and pressure not only influence the partial pressure of SiO above the free melt surface, but also the near surface melt convection which, in turn, influences the near surface oxygen concentration gradient. Although, notable progress has been achieved in recent years, the quantitative prediction of the incorporated oxygen content needs further improvements.

If magnetic fields are applied, additional terms and equations have to be included in the calculations. In case of AC fields, mean values of the Lorentz force are used, which are described by the product of the alternating field and the alternating current induced in the melt. These forces only depend on the frequency and the geometry of the coils and the melt volume, but are independent of melt velocities. For DC fields, on the other hand, the Lorentz force depends on the melt flow velocity which adds an equation of the electric potential due to the interaction of the steady magnetic field and the melt velocity. With respect to the standard turbulence model, the Lorentz force suppresses the mean melt flow velocity and, thus, less turbulence is generated. As velocity fluctuations which are modelled by the turbulent energy k are also directly damped, it has been proposed to add a negative term for turbulence generation to the k-equation which is proportional to the square of the magnetic field [27]. Although, this resulted in an improved predictability of the melt flow, the calculated interface shapes are not always in quantitative agreement with the experimental data (Fig. 7).

1.4. Verification of simulation results. The development of efficient and accurate simulation codes and the selection of the appropriate turbulence model are not possible without verification of the respective calculation results. As liquid silicon is non-transparent to light as well as highly reactive and has a melting point of 1412°C, it is not feasible to carry out direct flow measurements. The only possibility are temperature measurements with thermocouples encapsulated in silica [38] or light wave guides made of silica [11]. These techniques work rather well and are established tools to investigate silicon melts. If two or more of these temperature sensors are introduced into the melt, time correlated temperature measurements allow for a rough estimation of the convection pattern [39]. The theoretically predicted baroclinic waves in the outer melt volume whose behav-

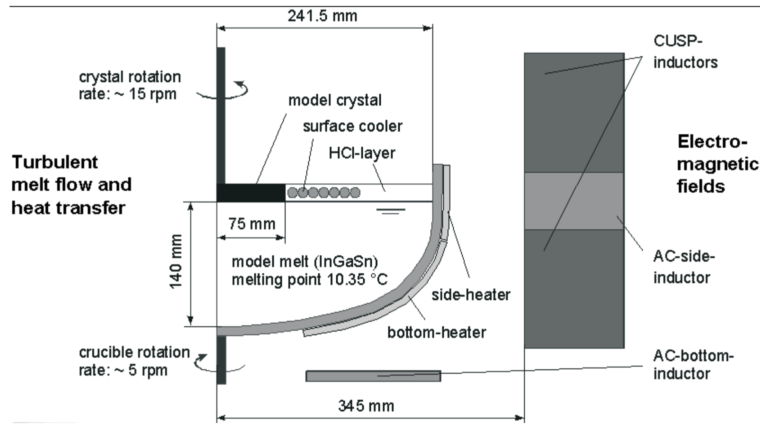

Fig. 8. Laboratory setup for experimental modelling of CZ growth processes with InGaSn as a model melt [26].

ior strongly depends on crucible rotation have been successfully investigated and verified by this method [40, 41, 42, 43].

Unfortunately, the obtained information from temperature measurements in the melt volume is not sufficient for a reliable test of new or modified simulation codes. In addition, the costs for real growth experiments are very high. A promising alternative are experiments with metals or metal alloys which are liquid at room temperature. A preferred candidate is an eutectic InGaSn alloy with the melting point of 10.35°C [44]. The parameters of these experiments are chosen such that the various dimensionless numbers (Reynolds, Rayleigh, Hartmann, Prandtl) are as similar as possible to silicon growth conditions in CZ pullers. It can be shown that the results of such a model system can indeed serve as a reference for comparing simulation results and can also physically reproduce the respective situation of a real growth process. A typical laboratory setup for a 20" crucible filled with InGaSn is shown in Fig. 8. The growing crystal is represented by a rotating plate which is strongly cooled in order to simulate the heat flux through the growth interface. The surface cooler above the InGaSn melt accounts for the radiation heat loss at the melt surface. Various heaters at the crucible wall and bottom provide the necessary heat flux through the crucible/melt interface to reproduce the effect of the heating system in real CZ pullers. The setup has also been equipped with different magnetic field configurations – static as well as dynamic fields and combined fields. The temperature is measured by thermocouples and the velocity components of the melt flow are determined by a conductive anemometer. A great advantage of this experimental setup is the possibility to derive thermal boundary conditions along various interfaces in a rather direct way with no need to perform any global or even integrated heat transfer calculations. Moreover, these experiments are much cheaper and can be carried out much faster than the growth of real silicon crystals. Numerous magnetic field configurations were thus economically and efficiently investigated that was extremely helpful in selecting the most favorable configuration for silicon crystal growth.

2. Floating zone crystal growth.

2.1. Electromagnetic fields in FZ crystal growth. There are principally two different concepts for the floating zone technique (Fig. 9). One is the pedestal method, where a poly silicon rod is inductively melted at its upper end by a high frequency (HF) coil (Fig. 9*a*). Typical frequencies are 1–4 MHz. Crystals grown by this method are limited to a maximum diameter of ca. 10–20 mm as the liquid bridge between the poly silicon rod and the growing crystal cannot be

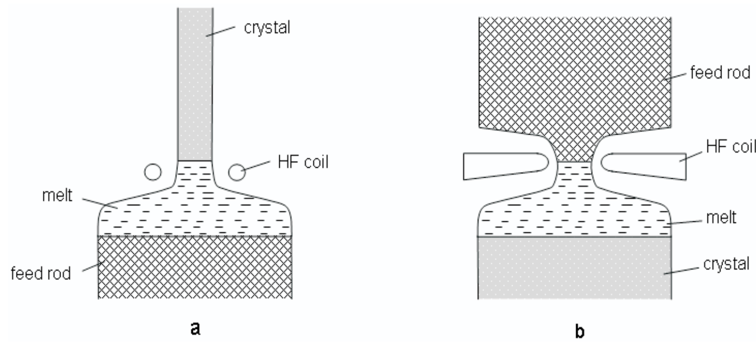

Fig. 9. Floating zone (FZ) growth process: pedestal technique (*a*), needle eye technique (*b*).

maintained for larger diameters. The so-called needle-eye technique overcomes the above diameter limitation (Fig. 9*b*). The lower end of a poly silicon rod is inductively melted by a pancake shaped one-turn HF coil. The melt flows through a central hole (needle eye) of the coil down onto the growing crystal below the coil.

Magnetohydrodynamical effects of the HF field are essentially relevant in the bulk and the surface of the melt cap while the layer of molten silicon at the lower end of the poly rod is so thin that pronounced convection patterns are suppressed. The use of static and dynamic fields has also been investigated for the FZ processes [45, 46, 47, 48] and their impact on the melt flow in the cap was studied in detail [49]. The basic effects of these fields on the melt convection are principally the same as for the CZ processes, but, due to the much smaller melt volume and the HF field, the melt flow is not comparable.

2.2. Challenges in FZ crystal growth. The most important part of the FZ puller is the HF coil. The coil design must ensure that the poly silicon rod is homogeneously melted at its lower end and that the melt cap is simultaneously stabilized and the crystal grows with a cylindrical shape. The larger the crystal diameter, the more difficult it is to meet both requirements. The biggest challenge is that these requirements apply for the entire growth process starting from the Dash neck with a 3 mm diameter to the full crystal diameter of up to 200 mm. This means that tight control of the growth process by the HF field has to be achieved under enormously changing geometrical conditions. Although, the well established one-turn coil with its pancake shape and the central hole is still the standard design, the specific details and the precise manufacturing of the coil are of utmost importance. For example, deviations of a few tenths of a millimeter from the calculated shape at the central hole can result in a complete process failure. Consequently, the proper design of the HF coil is rather involved and most challenges of FZ growth are related to this issue. In contrast to the CZ crystal growth, the main effect of the electromagnetic field is the inductive heating of the poly rod and the melt cap of the growing crystal. Furthermore, the generated electromagnetic forces are important to stabilize the shape of the melt cap.

The technologically most relevant quality parameter of FZ crystals is a homogeneous resistivity profile, both in axial and radial directions. One also has to distinguish between macroscopic (several mm scale) and microscopic (below 1 mm scale) inhomgeneities. While the axial macroscopic resistivity variation is adjusted by tight control of the gas doping system (either B_2H_6 or PH_3 are common as dopants), the macroscopic radial dopant profile is strongly influenced by the generated convection pattern in the melt cap. For small diameters, thermocapillary (Marangoni) forces have a major effect on the melt flow even in the bulk of the melt volume, while for larger crystal diameters (> 50 mm), as they are

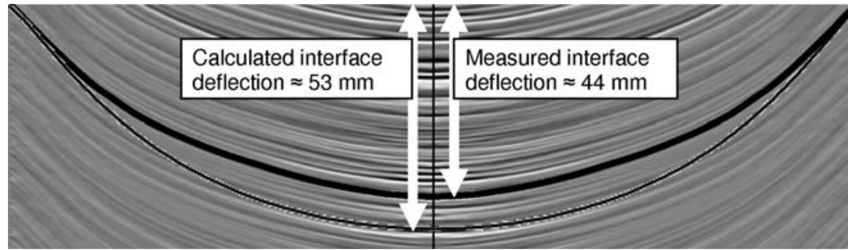

Fig. 10. Comparison of a simulated shape of the growth interface with experimental data (photoscanning measurement) for a 200 mm FZ growth process.

common in industrial FZ growth processes, they mainly have an influence at the crystal rim. Nevertheless, owing to the relatively small melt volume if compared to CZ, the Marangoni effects cannot be neglected even for larger crystal diameter. Besides buoyancy and centrifugal forces – the latter is of course dominated by crystal rotation schemes – the melt convection is also driven by the HF field of the coil [49, 50]. Thus, the relative shift of the crystal axis versus the center of the coil and the coil design itself are strongly impacting the radial dopant distribution. Interestingly, the poly rod rotation rate has a notable influence, too, although the rotation rate is usually very slow and the diameter of the melt neck ranges only from 10 to 20 mm. Static magnetic fields have been applied in vertical and horizontal directions with field strengths as high as 5 Tesla [46]. It was reported that an axial field of several 100 G significantly worsened the macroscopic radial resistivity profile, while rotating magnetic fields improved it. Microscopic resisivity variations (the so- called striations), on the other hand, which are related to the time dependent convection pattern and, as a consequence, generate local growth rate fluctuations, are found to be suppressed by static axial magnetic fields of several 100 G. At a higher field strength, however, they reappeared again [46]. The rotating field was also reported to reduce striations [48]. In conjunction with its favorable effect on the macroscopic profile, it is, therefore, preferred to static fields. It should be noted that striations are otherwise difficult to control by standard growth parameters like crystal rotation, etc., or by the coil design, as these parameters do not seem to act on the time dependence of the local melt flow near the growth interface. Unfortunately, data on radial dopant distributions under the influence of magnetic fields are rare for FZ crystals and often only apply to very small crystal diameters which are not standard in the industry.

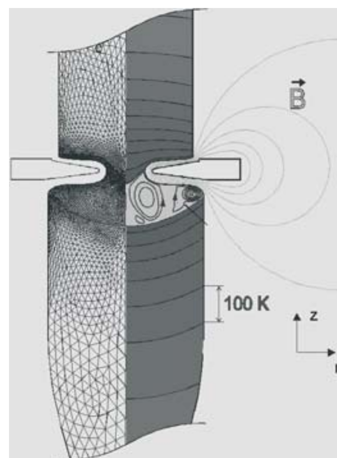

Fig. 11. Simulation of FZ growth process.

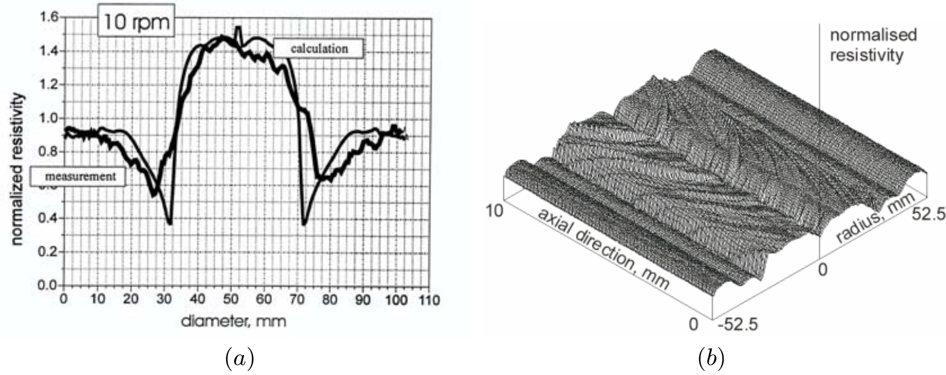

(a) (b)

Fig. 12. (*a*) Comparison of a simulated radial resistivity profile with experimental data for a 100 mm FZ growth process (crystal rotation 10 rpm). (*b*) Simulated resistivity distribution in a vertical cross-section of a FZ crystal (3D steady-state calculations).

2.3. Simulation of HF field and melt convection of FZ processes. Although the depicted process in Fig. 9 suggests a radial symmetry, the gap between the two electrodes which feed the HF power to the coil indeed introduces a strong local field asymmetry. A detailed study of the HF electromagnetic forces and their effect on the melt flow in the cap revealed that the counteraction of electromagnetic and Marangoni forces, which are of the same order of magnitude but have opposite directions at the melt cap surface, produce melt flow patterns that are sensitive to the 3D shape of the inductor coil [50]. Thus, 3D calculations are necessary to obtain accurate results. It has been shown that the asymmetry of the inductor is also the root cause for the rotational resistivity striations in the grown crystal [51, 52].

Due to the relatively small melt volume, the turbulence situation is quite different if compared to CZ, and usually a laminar time-dependent flow model is assumed [52]. The small geometrical dimensions also keep the number of grid cells at a level which allows for simulations of reasonable computation times.

Another issue is the calculation of the shape of the molten zone. The state-of-the-art phase boundary calculations for industry-size FZ processes are based on a 2D approximation, however, taking into account the 3D properties of the inductor [53]. Although the overall calculated 2D shapes of phase boundaries mostly fit well to the experimental observations, the results are not always satisfactory. As can be seen in Fig. 10, the calculated shape of the growth interface quantitatively deviates from the experimental results. This is attributed to the fact that the calculations of the melt convection and of the phase boundaries were not yet coupled, but carried out separately. Contrary to CZ, simulation results of FZ processes have been reported rather seldom. Nevertheless, the state-of-the-art of these calculations is remarkable. The current capability of available codes (Fig. 11) does not only allow to calculate the HF field and the electromagnetic forces exerted on the surface of the melt cap, but they can also simulate the strongly time dependent melt flow inside the melt cap. A real highlight is the correct prediction of the radial resistivity profile (Fig. 12*a*) and rotational striations (Fig. 12*b*) as a function of the coil geometry and various growth parameters. Even statistical fluctuations of these profiles with the crystal length can be simulated [54]. This has tremendously contributed to savings in time and costs of FZ development activities.

Further development of the numerical codes focuses on the calculation of transient FZ process phases, i.e., the seed- and end-cone growth as well as the impact of inductor power variations during the growth process [55].

Acknowledgement. The authors are greatly indebted to E.Tomzig, Th.Wetzel, P.Fuchs, G.Ratnieks, E.Dornberger, A.Sattler, O.Gräbner, A.Mühe, G.Raming, B.Hanna, V.V.Kalaev for their help and contribution to this research work.

REFERENCES

1. H.A. Chedzey, D.T. Hurle. *Nature*, vol. 239 (1966), p. 933.
2. H.P. Utech, M.C. Flemings. *J. Appl.Phys.*, vol. 37 (1966), p. 2021.
3. A.F. Witt, C.J. Herrman, H.C. Gatos. *J.Mat.Sci.*, vol. 5 (1970), p. 822.
4. K. Hoshi, T. Suzuki, Y. Okubo, N. Isawa. Abstract 324. In *The Electrochemical Society Extended Abstracts*, vol. 80–1, (1980) p. 811.
5. T. Suzuki, N. Isawa, Y. Okubo, K. Hoshi. In *Semiconductor Silicon 1981* (Ed. H.R. Huff, R.J. Kriegler, Y. Takeishi, The Electrochemical Society, Pennington NJ, (1981), p. 90.
6. S. Takasu, K. Homma, E. Toji, K. Kashima, M. Ohwa, S. Takahashi. *PESC'88 RECORD*, vol. April 1988 (1988), p. 1339.
7. A.M. Eidenzon, N.I. Puzanov. *Inorganic Materials*, vol. 33 (1997), no. 3, p. 272.
8. J.G. Park, H.K. Chung. In *Silicon Wafer Symposium SEMICON West 99* (SEMI 1999, D–1).
9. R. Falster. In *Silicon Wafer Symposium SEMICON West 99* (SEMI 1999, E–13).
10. J. Czochralski. *Z. Phys. Chem*, vol. 92 (1918), pp. 219.
11. O. Gräbner, A. Mühe, G. Müller, E. Tomzig, J. Virbulis, W.V. Ammon. *Material Science and Engineering*, vol. B73 (2000), p. 130.
12. V.V. Voronkov. *J. Crystal Growth*, vol. 59 (1982), p. 625.
13. N. Riley. *J. Crystal Growth*, vol. 85 (1987), p. 417.
14. J.A. Burton, R.C. Prim, W.P. Slitcher. *J. Chem.Phys.*, vol. 21 (1953), p. 1987.
15. R.W. Series, D.T.J. Hurle. *J. Crystal Growth*, (1991), p. 305.
16. R.W. Series, D.T.J. Hurle, K.G. Barraclough. *J. Appl. Math.*, vol. 35 (1985), p. 195.
17. P.S. Ravishankar, T.T. Braggins, R.N. Thomas. *J. Crystal Growth*, vol. 104 (1990), p. 617.
18. H. Hoshikawa, H. Konda, H. Hirata. *Japan J. Appl. Phys.*, vol. 23 (1984), p. L37.
19. R.W. Series. *J. Crystal Growth*, vol. 97 (1989), p. 85.
20. E. Iino, K. Takano, M. Kimura, H. Yamagishi. *Material Science and Engineering*, vol. B36 (1996), p. 142.
21. M. Oshima, N. Taniguchi, T. Kobayashi. *J. Crystal Growth*, vol. 137 (1994), p. 142.
22. K.S. Choe. *J. Crystal Growth*, vol. 262 (2004), p. 35.
23. M. Ohwa, T. Higuchi, E. Toji, M. Watanabe, K. Homma, S. Takasu. In *Semiconductor Silicon 1986* (Ed. H.R. Huff, T. Abe, B. Kolbesen, The Electrochemical Society, Pennington NJ, (1986), p. 117.
24. H. Hirata, K. Hoshikawa. *J. Crystal Growth*, vol. 96 (1989), p. 747.
25. R.W. Series. *J. Crystal Growth*, vol. 97 (1989), p. 92.
26. T. Wetzel, A. Muiznieks, A. Mühlbauer, Yu. Gelfgat, L. Gorbunov, J. Virbulis, E. Tomzig, W.V. Ammon. *J. Crystal Growth*, vol. 230 (2001), p. 81.
27. J. Virbulis, T. Wetzel, A. Muiznieks, B. Hanna, E. Dornberger, E. Tomzig, A. Mühlbauer, W.V. Ammon. *J. Crystal Growth*, vol. 230 (2001), p. 92.
28. V. Galindo, G. Gerbeth, W.V. Ammon, E. Tomzig, J. Virbulis. *Energy Conversion and Management*, vol. 43 (2002), p. 309.
29. R. Mössner, G. Gerbeth. *J. Crystal Growth*, vol. 197 (1999), p. 341.
30. W.C. Dash. *J. Appl.Phys.*, vol. 30 (1959), p. 459.
31. W.V. Ammon, E. Dornberger, P.O. Hansson. *J. Crystal Growth*, vol. 198/199 (1999), p. 390.
32. M. Mihelcic, K. Wingerath. *J. Crystal Growth*, vol. 97 (1989), p. 42.
33. H.J. Leister, M. Peric. *J. Crystal Growth*, vol. 123 (1992), p. 567.
34. C. Wagner, R. Friedrich. *Notes on Num.Fluid Mech.*, vol. 60 (1997), p. 36.

35. I.Y. Estratov, V. Kalaev, A. Zhmakin, Y.N. Makarov, A.G. Abramov, N.G. Ivanov, E.M. Smirnov, E.Dornberger, J.Virbulis, E.Tomzig, W.V. Ammon. *J. Crystal Growth*, vol. 230 (2001), p. 22.

36. I.Y. Estratov, V. Kalaev, V. Nabokow, A. Zhmakin, Y.N. Makarov, A.G. Abramov, N.G. Ivanov, E.A. Rudinsky, E.M. Smirnov, S.A. Lowry, E. Dornberger, J. Virbulis, E. Tomzig, W.V. Ammon. *Microelectronic Engineering*, vol. 56 (2001), p. 139.

37. T. Wetzel, J. Virbulis, A. Muiznieks, W.V. Ammon, E. Tomzig, G. Raming, M. Weber. *J. Crystal Growth*, vol. 266 (2004), p. 34.

38. S. Togawa, S.–I. Chung, S. Kawanashi, K. Izunome, K. Terashima, S. Kimura. *J. Crystal Growth*, vol. 160 (1996), p. 41.

39. A. Seidl, G. Müller, E. Dornberger, E. Tomzig, B. Rexer, W.V. Ammon. In *The Electrochem. Soc. Proceedings*, vol. 98–1 (1998), p. 417.

40. A. Seidl, G. McCord, G. Müller, H.–J. Leister. *J. Crystal Growth*, vol. 137 (1994), p. 326.

41. Y. Kishida, M. Tanaka, H. Esaka. *J. Crystal Growth*, vol. 130 (1993), p. 75.

42. P.A.C. Whiffin, T.M. Burton, J.C. Brice. *J. Crystal Growth*, vol. 32 (1976), p. 205.

43. C.D. Brandle. *J. Crystal Growth*, vol. 57 (1982), p. 65.

44. L. Gorbunov, A. Pedchenko, A. Feodorov, E. Tomzig, J. Virbulis, W.V. Ammon. *Energy Conversion and Management*, vol. 257 (2003), p. 7.

45. P. Dold, A. Cröll, K.W. Benz. *J. Crystal Growth*, vol. 183 (1998), p. 545.

46. A. Cröll, F.R. Szofran, P. Dold, K.W. Benz, S.L. Lehoczky. *J. Appl. Phys.*, vol. 183 (1998), p. 554.

47. N. Ma, J.S. Walker, A. Lüdge, H. Riemann. *J. Crystal Growth*, vol. 230 (2001), p. 118.

48. P. Dold, A. CrRöll, M. Lichtensteiger, T. Kaiser, K.W. Benz. *J.Crystal Growth*, vol. 231 (2001), p. 95.

49. G. Raming, A. Muiznieks, A. Mühlbauer. *J. Crystal Growth*, vol. 230 (2001), p. 108.

50. G. Ratnieks, A. Muižnieks, L. Buligins, G. Raming, A. Mühlbauer. *Magnetohydrodynamics*, vol. 35 (1999), no. 3, p. 223.

51. G. Ratnieks, A. Muižnieks, L. Buligins, G. Raming, A. Mühlbauer, A. Lüdge, H. Riemann. *J. Crystal Growth*, vol. 216 (2000), p. 204.

52. G. Ratnieks, A. Muižnieks, A. Mühlbauer, G. Raming. *J. Crystal Growth*, vol. 230 (2001), p. 48.

53. G. Raming, A. Muiznieks, A. Mühlbauer. *J. Crystal Growth*, vol. 255 (2003), p. 227.

54. A. Mühlbauer, A. Muižnieks, G. Raming, H. Riemann, A. Lüdge. *J. Crystal Growth*, vol. 198/199 (1999), p. 107.

55. A. Rudevics, A. Muižnieks, G. Ratnieks, A. Mühlbauer, Th. Wetzel. *J. Crystal Growth*, vol. 266 (2004), p. 54.